Surface & Coatings Technology 393 (2020) 125762

Contents lists available at ScienceDirect

Surface & Coatings Technology

journal homepage: www.elsevier.com/locate/surfcoat

How microalloying of the Al target can improve process and film characteristics of sputtered alumina

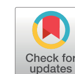

B. Kohlhauser[a,b], H. Riedl[a], C.M. Koller[a], V. Paneta[c], S. Kolozsvári[d], P.H. Mayrhofer[a,*]

[a] *Institute of Materials Science and Technology, TU Wien, A-1060 Vienna, Austria*
[b] *AC2T Research GmbH, A-2700 Wiener Neustadt, Austria*
[c] *Department of Physics and Astronomy, Uppsala University, SE-75120 Uppsala, Sweden*
[d] *Plansee Composite Materials GmbH, D-86983 Lechbruck am See, Germany*

ARTICLE INFO

Keywords:
Micro-alloying
Al_2O_3
Target hysteresis
Target poisoning
Transition metals
Mechanical properties

ABSTRACT

The outstanding thermo-mechanical and chemical stability of Al_2O_3 thin films attracts particular attention in academia and industry. Here we show that alloying of the powder metallurgically prepared Al targets with 2 as well as 5 at.% of Cr, Mo, or W significantly improves the process stability (e.g., reducing arcing events) for Al_2O_3, allowing their reactive magnetron sputtering in DC mode (substrate temperature was always 360 °C). Contrary to these microalloying elements, Nb did not change or improve the process characteristics of the Al target due to the relatively coarse Nb particles (< 125 µm). Particularly the small (< 10 µm) and fine-dispersed W particles are very effective in stopping the collision cascades to concentrate them to the near subsurface target-regions. This leads to a shift of the target-poisoning onset from O_2/(Ar + O_2) flow-rate-ratios of about 32 to 52%, specifically when adding 5 at.% to the Al target. Thereby also improved deposition rates are possible.

However, detailed X-ray diffraction (XRD) and transmission electron microscopy studies show that only thin films developed from the 2 at.% W alloyed Al target have a nanocrystalline γ-Al_2O_3-based structure comparable to those prepared from Al or Cr alloyed Al targets. The films are with 28.3 GPa instead of 26.8 GPa slightly harder when sputtered from $Al_{0.98}W_{0.02}$ instead of Al targets. Higher W contents (and also Nb) in the target lead to the formation of Al_2O_3-based films with considerably lower crystalline phase fractions and hardness (~13 GPa). Hardest films, with 30.0 and 29.6 GPa, are obtained when using $Al_{0.98}Cr_{0.02}$ and $Al_{0.95}Cr_{0.05}$ targets, respectively. The formation of volatile Mo-oxides during film growth interferes the structure development, leading to rather soft films with 8.0 GPa especially when using the higher Mo alloyed $Al_{0.95}Mo_{0.05}$ target.

Based on our results we can conclude that microalloying the Al targets with small and fine-dispersed Cr or W particles not just improves process stability and deposition rate during reactive sputtering of Al_2O_3, but also their mechanical thin film properties.

1. Introduction

Alumina thin films have spread to many fields of applications ranging from optical applications [1], corrosion protection [2], diffusion barriers [3,4], to machining tools [5,6]. They are in demand because of their electronic structure, high hardness (even at high temperatures), thermal as well as chemical stability, and their low interaction with working materials [6–8]. Initially, alumina thin films were predominantly produced via chemical vapor deposition (CVD), as the high process temperatures allowed the formation of the thermodynamically stable structure, α-Al_2O_3. Since the early achievements with reactive magnetron sputtering in the 1990s [9–11], the individual physical vapor deposition (PVD) processes have been improved tremendously allowing to produce high quality crystalline γ-Al_2O_3 thin films. Although it is possible to deposit α-Al_2O_3 by sputtering at high deposition temperatures [11–13], also the metastable γ-Al_2O_3 is a reasonably good alternative accessible already at lower temperatures (thus suitable for a larger variety of substrate materials).

For high deposition temperatures, particular during CVD, the low thermal expansion of α-Al_2O_3 often leads to severe crack formation during the post-process cooling [6]. PVD coatings on the other side can be prepared at much lower temperatures [14], reducing the thermally induced strains and often exhibit even compressive stresses. This gives PVD Al_2O_3 thin films an enhanced fatigue and thermal shock resistance [15], making them attractive for machining applications [6]. However, in order to form hard crystalline films by PVD, a threshold energy at the

* Corresponding author.
E-mail address: paul.mayrhofer@tuwien.ac.at (P.H. Mayrhofer).

https://doi.org/10.1016/j.surfcoat.2020.125762
Received 25 February 2020; Received in revised form 4 April 2020; Accepted 9 April 2020
Available online 13 April 2020
0257-8972/ © 2020 The Authors. Published by Elsevier B.V. This is an open access article under the CC BY-NC-ND license
(http://creativecommons.org/licenses/BY-NC-ND/4.0/).

substrate surface has to be surpassed, allowing for sufficient surface diffusion [7]. This is reflected by the influence of the substrate temperature as well as the applied bias potential on the thin film crystallinity [8]. So far, no commercially viable solution to form PVD α-Al_2O_3 at low deposition temperatures has been found and research focuses on the improvement of γ-Al_2O_3 thin films.

The inherently unstable reactive deposition process of alumina, due to the poisoning of the Al target, is an extremely important research task as well. The running-mode of the Al target during reactive magnetron sputtering in Ar/O_2 gas mixtures (to form Al_2O_3) can be divided into three regimes [7,16]. In the metallic mode regime, at low oxygen partial pressures, typically no Al-oxide islands or continuous Al-oxide layer is formed at the target-surface. Under these conditions, metallic to sub-stoichiometric oxide thin films are produced with high deposition rates. Operating the target in the so-called poisoned mode regime, at higher oxygen partial pressures, non-conductive Al_2O_3-based islands and even continuous layers may form at the target-surface. This immediately changes the electric conductivity of the target-surface, secondary electron emission, as well as the sputter yield. Because, now a ceramic has to be sputtered, and in the case of Al_2O_3 even a non-conductive one. Aside from very low deposition rates (lower than what would be expected according to the sputter yields [17]) the resulting thin films are typically amorphous and exhibit weak mechanical properties [7]. Between these regimes is a transition regime, which allows for the deposition of γ-Al_2O_3 coatings with good mechanical properties but typically at low deposition rates. Unfortunately, the transition regime is characterized by generally unstable conditions due to arcing-events as a result of nonconductive Al_2O_3 formation at the target-surface [18].

Many strategies to overcome the unwanted process instability due to the hysteresis effect [19] rely on complex feedback controls to adjust the availability of oxygen [20–23]. Furthermore, high gas flows coupled with increased pumping speeds or specific target designs can influence the sputter erosion areas [20,24]. Most of these strategies do not consider or even reduce the already very low deposition rates caused by the target-poisoning effects [22,25].

A very promising approach to stabilize the transition regime of operating the Al targets was outlined by Berg et al. and relies on the doping of the target surface with heavy elements (e.g. Pt) utilizing a serial secondary sputter source [26]. This doping effect enhances the collision cascade of impinging Ar ions at the target surface and reflects the cascading light Al atoms back towards the surface [27] in a kind of rebound effect. Monte Carlo based modeling studies (TRIDYN) by Kubart et al. have shown that these effects can also be achieved with other elements such as W [28]. Simulations promise an increase of the deposition rate of up to 80% when the Al target is doped with W [29], which has been confirmed experimentally [30]. The W-doped Al targets were obtained by sputtering W onto Al targets. Similar theoretical studies also suggest that an amplification of the sputter yield occurs if Al targets are doped with heavy elements [31]. The formation of non-conductive Al_2O_3 islands at the cathode surface is also a problem during arc evaporation for Al_2O_3-based films, where the addition of Si to Al-based cathodes proved to be beneficial [32].

In order to reduce the complexity of the deposition process itself, and still allow for the amplification effects, we study how Cr, Mo, W, or Nb microalloyed Al targets (powder metallurgically produced) influence the DC reactive magnetron sputtering process of Al_2O_3 and their thin film characteristics (such as chemical composition, growth morphology, and mechanical properties).

2. Experimental

We used an ultra-high vacuum (UHV) laboratory scale unbalanced magnetron sputtering system (Orion 5, AJA), equipped with a 3-inch target (Plansee Composite Materials), for investigating the process conditions as well as to develop Al_2O_3-based films with 2 at.% as well as

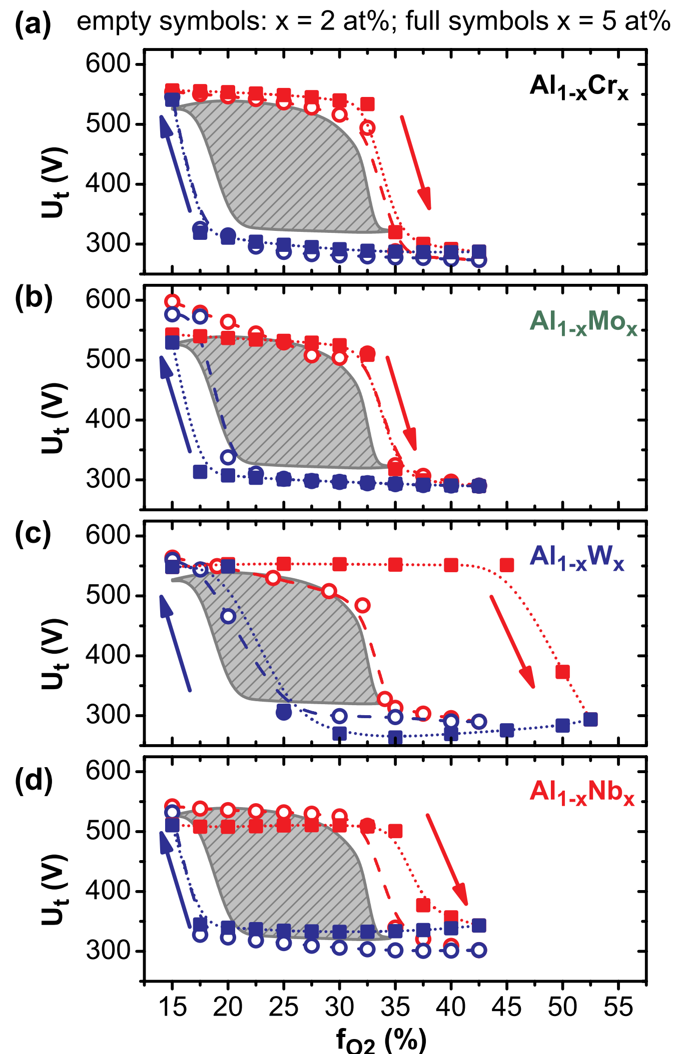

Fig. 1. U_t-vs-f_{O2} hysteresis (the values for the target-potential U_t are negative) of the (b) $Al_{1-x}Cr_x$, (c) $Al_{1-x}Mo_x$, (d) $Al_{1-x}W_x$, and (e) $Al_{1-x}Nb_x$ targets with 2 at.% (empty symbols) and 5 at.% (full symbols) alloying content. The gray shaded area shows the hysteresis curve of the unalloyed Al target.

5 at.% Cr, Mo, Nb, or W alloyed Al targets. The $O_2/(Ar + O_2)$ flow-rate-ratios (f_{O2}) of the $Ar + O_2$ gas mixture (both with 99.999% purity) was varied between 0 and 55% (with a constant $Ar + O_2$ flow-rate of 20 sccm, which results in a working gas pressure of ~0.4 Pa) while operating the targets with a DC power density of 9 W·cm^{-2}. We recorded and analyzed the target-potential (U_t) versus f_{O2} (U_t-vs-f_{O2}) hysteresis curve for the transition and poisoned mode regimes of the target-operation. The subsequent development of coatings was conducted with f_{O2} conditions at the transition regime (for increasing f_{O2}), which varies with the microalloyed target (we used $f_{O2} = 31\%$ for all targets except the W-alloyed ones for which we used $f_{O2} = 38\%$). The microalloyed targets (density above 99.8%) were produced by powder metallurgy of fine-grained Al powders (particle size < 63 µm) mixed with Cr, Mo, Nb, or W powders. These particles (particle size for Cr < 80 µm, Mo < 30 µm, W < 10 µm, and Nb < 125 µm) are evenly distributed across the target volume with a fraction to have 2 as well as 5 at.% microalloyed $Al_{1-x}TM_x$ targets, with TM ∈ {Cr, Mo, Nb, W} and x ∈ {0.02, 0.05}. The alloying elements were selected based on their mass (atomic masses in Dalton are Al: 26.98, Cr: 52.00, Nb: 92.91, Mo: 95.94, W: 183.85) as well as their ability to stabilize the corundum structure. Specifically Cr_2O_3, which crystallizes in the corundum type structure, is known to form a solid solution with Al_2O_3 [33–35] and stabilizes its

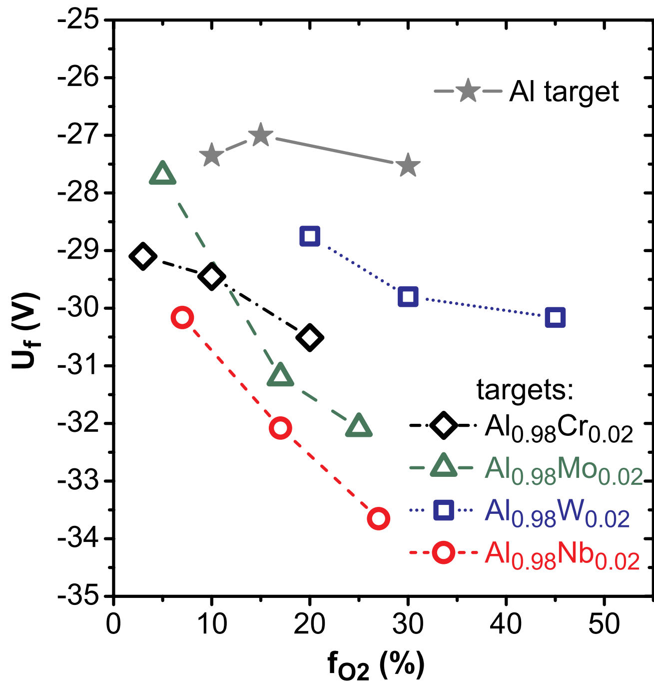

Fig. 2. Floating potential U_f based on Langmuir wire probe measurements during sputtering the unalloyed Al target and the $Al_{0.98}Cr_{0.02}$, $Al_{0.98}Mo_{0.02}$, $Al_{0.98}W_{0.02}$, and $Al_{0.98}Nb_{0.02}$ targets at various f_{O2} values.

corundum type structure.

The substrate heater was set to 500 °C resulting in an actual substrate temperature of 360 ± 10 °C (obtained by calibrating standards) and the substrates (100-oriented Si platelets, 20.0 × 7.0 × 0.45 mm^3) were biased with an asymmetric bipolar pulsed (150 kHz, 1296 ns) DC potential of −50 V. For sputtering and biasing, RPG 50 (MKS Instruments) generators with implemented arc detection and control units were used. Prior to loading the substrates to the chamber, they were cleaned in an ultrasonic acetone and ethanol bath for 10 min each. After reaching a base pressure of ≤0.5 mPa they were Ar-ion etched for 10 min with −700 V DC at an Ar gas pressure of 6 Pa. Simultaneously the target was sputter-cleaned behind a shutter using the same sputtering conditions as used for the deposition itself. The target-to-substrate distance was 85 mm and the deposition time was adjusted to have always around 1 µm thin films. The deposition rate is part of our results and depends on the target and f_{O2} used.

To investigate the effect of the microalloying elements on the plasma conditions, we used a standard Langmuir wire probe (ESPion, Hiden), which is mounted in an adapted Z400 sputtering system (Leybold Heraeus) 5 cm above the target-racetrack. For these measurements we used the same cathode, targets, and generators (unfortunately it was not possible to install the wire probe to the above-mentioned AJA system used for developing the coatings). However, these measurements are still valid for a qualitative characterization of the effect of microalloying elements on the plasma conditions. The measurements were recorded for different f_{O2} values [36].

The growth morphology of our coatings was studied by electron microscopy (SEM, FEI Quanta 250 FEG) and those coatings prepared from the 2 at.% alloyed targets were also studied by transition electron microscopy (TEM) using a FEI TECNAI F20 with an acceleration voltage of 200 kV and equipped with an Apollo XLTW SDD EDAX detector. Phase analyses were conducted with selected area electron diffraction (SAED). In addition to energy dispersive X-ray spectroscopy (EDS), the chemical composition was also determined by time-of-flight elastic recoil detection analysis (ToF-ERDA) using the 5 MV pelletron tandem accelerator at Uppsala University [37]. Measurements employed a 36 MeV I^{8+} primary ion beam and a ToF-telescope combined with a segmented gas ionization chamber located at a recoil detection angle of 45° [38]. Chemical compositions were evaluated as described in [39].

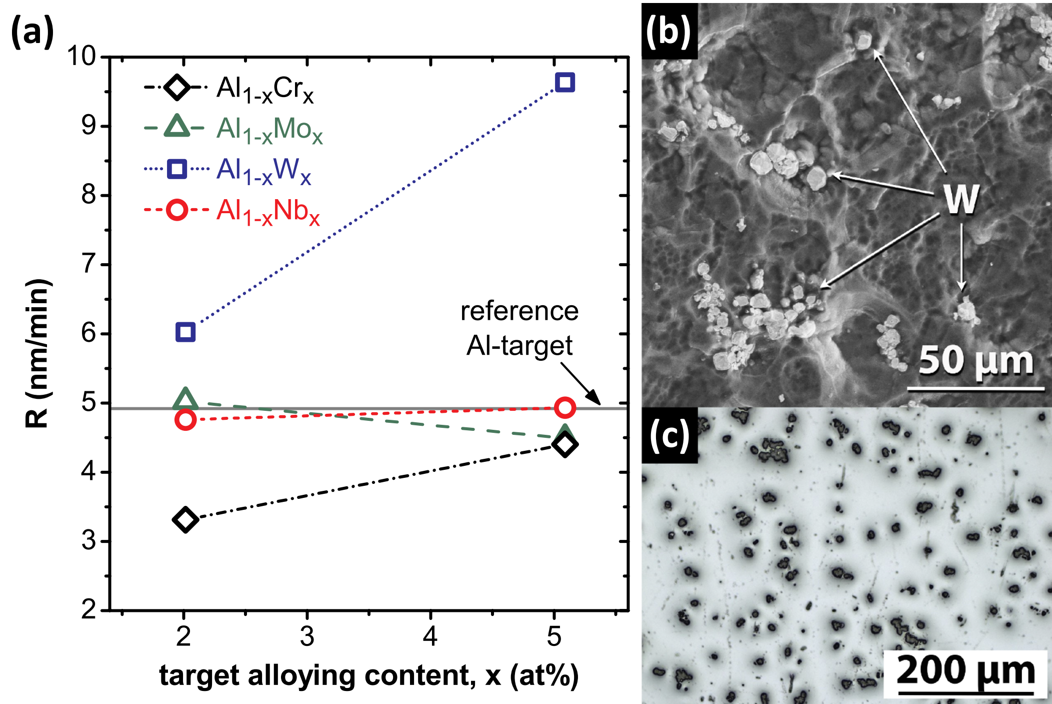

Fig. 3. (a) Deposition rate (R) for the individual microalloyed targets operated deep inside the transition regime (f_{O2} = 38% for the $Al_{1-x}W_x$ targets and 31% for the others). (b) SEM top view image of the $Al_{0.95}W_{0.05}$ target after the sputtering process with f_{O2} = 38% (specifically the target regions around the heavy and fine distributed W particles are sputtered with a higher rate, leading to the formation of exposed W particles). (c) Light optical microscopy top view image of the fresh unused $Al_{0.95}W_{0.05}$ target (with a slightly polished surface).

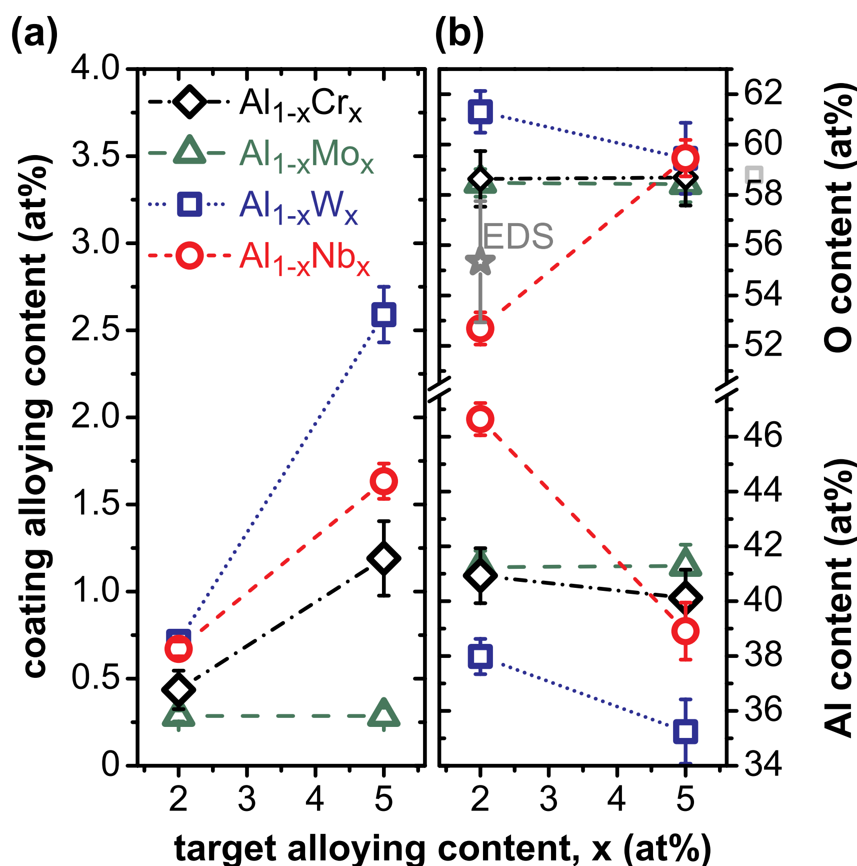

Fig. 4. (a) ERDA obtained element contents within the coatings prepared with $Al_{1-x}Cr_x$, $Al_{1-x}Mo_x$, $Al_{1-x}W_x$, and $Al_{1-x}Nb_x$ targets with 2 and 5 at.% alloying content (f_{O2} = 38% for the $Al_{1-x}W_x$ targets and 31% for the others). Ideally, for an Al_2O_3-based sesquioxide the oxygen content would be 60 at.%, thus the metal-fraction of the alloying elements within the coating is 2.5-times (=1/0.4) of the coating alloying content. (b) Oxygen and Al content of our Al_2O_3-based coatings. As expected, the O content is lower when using EDS.

X-ray diffraction (XRD) was conducted for detailed phase and structure analyses, utilizing a multipurpose diffractometer (Empyrean, Panalytical) in grazing incident (GI-XRD) setup (incident beam at 2°). The system was equipped with a Cu-K_α radiation source, a parallel beam mirror, as well as a scintillation detector (behind a 0.18° parallel plate collimator). To investigate any preferred growth orientations, the coatings were also analyzed in a Bragg-Brentano geometry with a Bragg-Brentano HD mirror and a PIXcel3D detector (Panalytical).

Mechanical properties, hardness (H) and indentation modulus (E), of our Al_2O_3-based thin films on Si substrates were characterized by nanoindentation, using an ultra-micro-indentation system (UMIS) equipped with a Berkovich tip. For each measurement, 40 indentation curves were analyzed according to the Oliver and Pharr method [40]. The residual stresses were calculated via the Stoney equation from the curvature of coated Si substrates (measured with a PS50, Nanovea), provided that several conditions summarized in [41] are fulfilled.

3. Results and discussion

The Cr, Mo, and W microalloyed Al targets show particularly at higher O_2 flow-rate-ratios f_{O2} substantially better process stability than the non-alloyed or the Nb microalloyed Al targets. Whereas severe arcing events are drastically reduced by the three microalloying elements Cr, Mo, and W, minor arcing events are only markedly reduced by Cr. These minor arcing events are not detected by the generator but qualitatively characterized by visual inspection of the process through a window. All four microalloying elements lead to a later (higher f_{O2} values) onset of the poisoning regime than obtained for the unalloyed Al target, Fig. 1. While this is only shifted slightly to higher f_{O2} values (from ~32 to ~35%) when alloyed with Cr or Mo (Fig. 1a and b), a pronounced shift to even 52% is obtained for the 5 at.% W alloyed Al target, Fig. 1c. The effect of Nb is between these extremes, Fig. 1d.

These results suggest that the heavy microalloying element particles within the Al target locally act as rigid regions. Thereby, the collision cascade in the target is concentrated to the near subsurface target-regions [26,30]. This leads to a higher energy-density, resulting in an enhanced deposition rate (R), which has also been observed for Ta, Ce, $CeSi_2$, or LaB_6 alloyed powder metallurgically prepared Ti-Al targets [42,43]. Consequently, also the target poisoning is shifted to higher f_{O2} values as any forming oxide layers are also effectively sputtered due to the now higher sputtering energy-density provided. The higher f_{O2} values before the target poisons – when alloyed with Cr, Mo, W, and Nb – allows for a wider process window to deposit stoichiometric Al_2O_3-based coatings.

Langmuir wire probe measurements show that the floating potential U_f is more negative when using the microalloyed Al targets instead of Al (Fig. 2). Operating the 2 at.% Mo, Cr, or Nb alloyed Al targets or the Al target at f_{O2} ~ 30% results in an ion density in the range $9–11 \cdot 10^{18}$ $1/m^3$. This increases to $16 \cdot 10^{18}$ $1/m^3$ when using the 2 at.% W alloyed Al target (also at f_{O2} ~ 30%). The higher ion density when using the W-alloyed target indicates that especially the small and heavy W-particles (evenly distributed in the Al target) effectively increase the sputter energy density. Through their repulsive effect that concentrates the collision cascades to near subsurface target-regions.

Based on these measurements (U_t-vs-f_{O2} hysteresis and Langmuir wire probe measurements) microalloying with W shows the most dominant effect on the Al target sputtering behavior and connected plasma conditions. Also, the deposition rate considerably increases when using the W microalloyed Al target compared to the other targets, Fig. 3a. The 5 at.% W alloyed target even allows for a deposition rate of 9.6 nm/min, which is 80% higher than that of the unalloyed Al target (indicated in Fig. 3a by the horizontal line at 4.9 nm/min), being in good agreement to theoretical studies [29,31] as well as approaches by co-sputtering [30].

During the discussion of Fig. 1 we envisioned that heavy particles evenly distributed in the target lead to a concentration of the sputtering

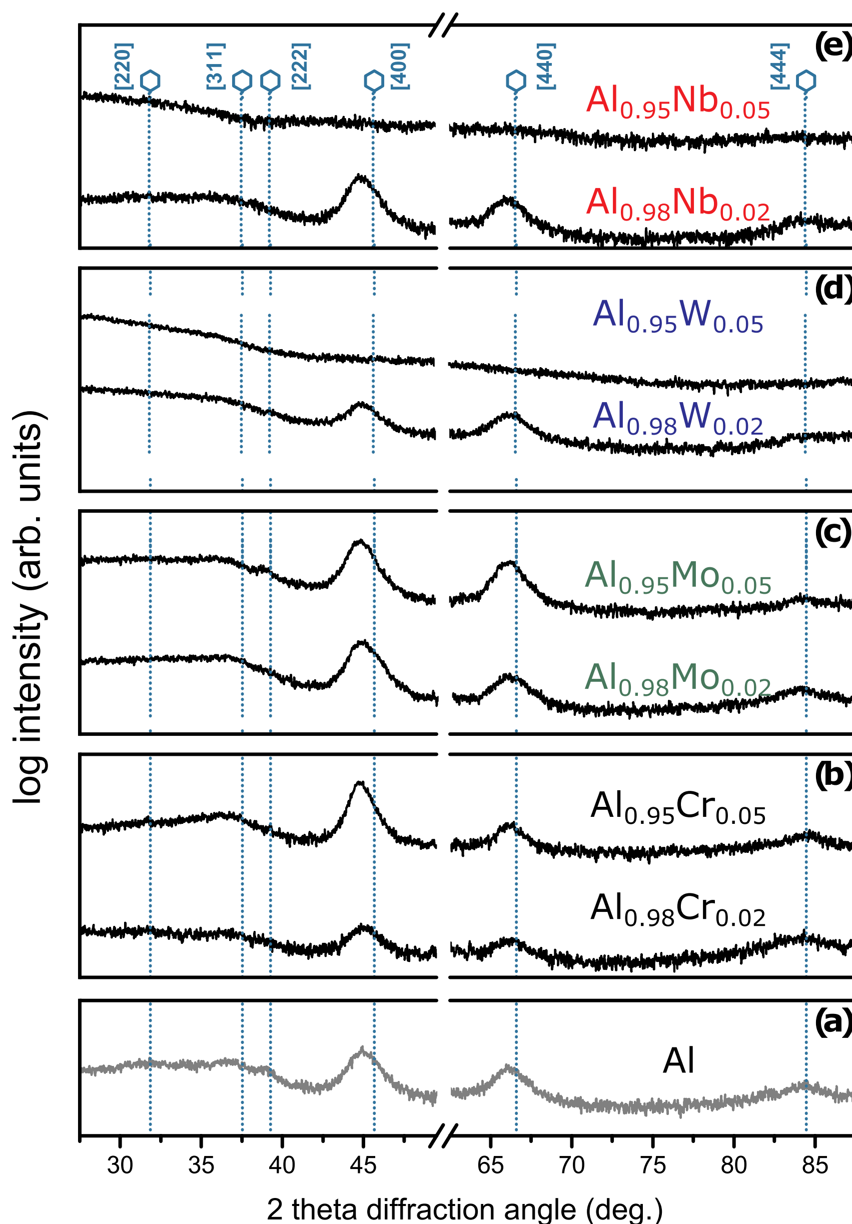

Fig. 5. GI-XRD measurements of our coatings prepared from an (a) unalloyed Al target, and (b) $Al_{1-x}Cr_x$, (c) $Al_{1-x}Mo_x$, (d) $Al_{1-x}W_x$, and (e) $Al_{1-x}Nb_x$ targets with 2 and 5 at.% alloying content (f_{O2} = 38% for the $Al_{1-x}W_x$ targets and 31% for the others). The XRD peak positions for γ-Al_2O_3 are indicated.

cascade to near subsurface target-regions. This in further consequence increases the sputtering energy per volume causing the substantial shift of the onset of the poisoning regime to higher f_{O2} values. This mechanism of an increased sputter rate through the collision-cascade barrier-feature (shortly: rebound effect) provided by the heavy particles is supported by top-view SEM investigations of a freshly sputtered $Al_{0.95}W_{0.05}$ target surface, Fig. 3b. The even distribution of small W particles in the target is clearly presented by the light optical microscopy overview image of an unused target (Fig. 3c). As a consequence of the condensed collision cascade (due to the heavy and fine-dispersed W particles, which act as a ram), the affected target regions sputter at a higher rate, leading to exposed W particles. The increased erosion around the W particles proves the rebound sputtering effect.

Consequently, the amplification in sputtering yield for these microalloyed targets is based on redirecting the collision cascade within the target towards their surface by collisions of the lighter target elements (Al) on the heavier W-particles. The ionization of the sputtered atoms as well as their contribution to sputtering is often considered negligible. The other microalloying elements, which are also much heavier than Al, do not show such a pronounced increase in deposition rate, which might be due to their considerably larger average particle size (see Experimental) and thus lower distribution density. This is in particular valid for the Nb particles, which are with < 125 μm more than 10-times larger than the W particles (< 10 μm).

The amount of the microalloying elements that are incorporated to the Al_2O_3-based coatings are presented in Fig. 4a based on ERDA and EDS measurements. Only traces of Mo are incorporated into the coating and their amount is the same whether using the 2 or the 5 at.% Mo alloyed target. This suggests that Mo, which easily forms volatile oxides, is removed by this process from the growth zone before its incorporation to the coating. A corresponding process may also be valid for Cr, which forms volatile oxides as well, but to a much lower extent. All microalloying elements are evenly distributed throughout the thickness of the coating. The oxygen content of all coatings (except for that prepared from the 2 at.% Nb alloyed Al target) is in the range 58–62 at.% and thus close to the sesquioxide stoichiometry of Al_2O_3,

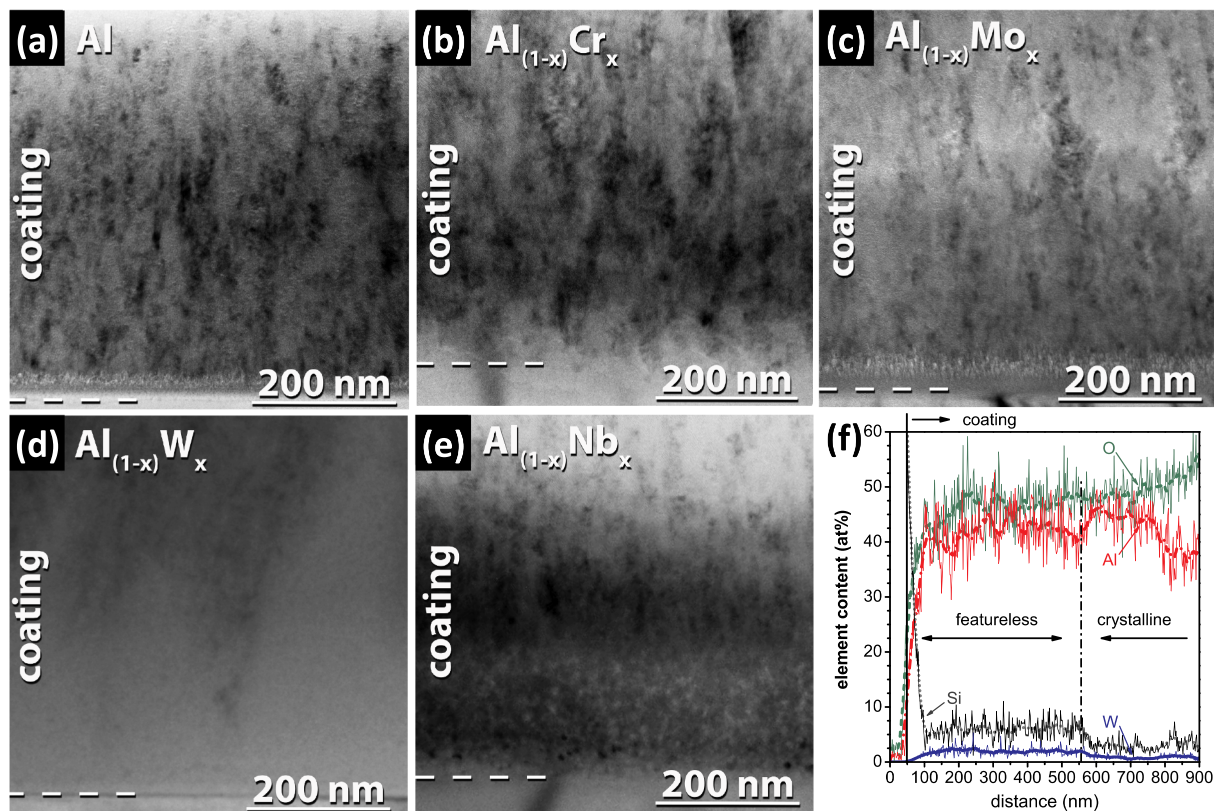

Fig. 6. Cross sectional TEM BF images of the interface near regions of our coatings prepared from an (a) unalloyed Al target, and (b) $Al_{0.98}Cr_{0.02}$, (c) $Al_{0.98}Mo_{0.02}$, (d) $Al_{0.98}W_{0.02}$, and (e) $Al_{0.98}Nb_{0.02}$ targets (f_{O2} = 38% for the $Al_{1-x}W_x$ target and 31% for the others). (f) TEM EDS line-scan across the substrate-near region of the coating prepared with the $Al_{0.98}W_{0.02}$ target.

Fig. 4b.

All crystalline coatings demonstrated a weak (100) orientation of their γ-Al_2O_3 crystallites, as detected during Bragg-Brentano XRD measurements. Their crystalline structure, characterized by GI-XRD, Fig. 5, strongly depends on the used target and the content of the microalloying elements. Using the Cr microalloyed targets results in the formation of coatings that are very similar in their XRD patterns to those obtained from the unalloyed Al target, because Cr easily incorporates into the Al_2O_3 lattice (compare Fig. 5a and b). As the Mo content within the coatings obtained from the Mo microalloyed targets is rather low, Fig. 4a, also their XRD pattern is rather similar to those obtained from the unalloyed Al target (Fig. 5c). W on the other hand (which is incorporated into the film) leads to decreasing XRD peak intensities with increasing W content, Fig. 5d. This might be a result of its electronic structure and preferred oxidation states, but the simple fact that W has roughly seven times the weight and six times the size of Al can also easily explain why concentrations below 1 at.% already have huge impacts on nucleation and growth mechanisms. Niobium, with a size comparable to W, exhibits a similar effect on the coating structure, Fig. 5e.

All coatings, except for those obtained from the Cr microalloyed target, exhibit a more or less pronounced featureless growth-morphology region at the Si substrate interface, indicating a rather high barrier for nucleation, Fig. 6a–d. The coatings obtained from the Mo microalloyed Al target and the unalloyed Al target (Fig. 6c and a) exhibit the development of a fine columnar growth structure after several nanometers of the initial featureless region. Contrary, the coatings obtained from the Nb and W microalloyed Al targets exhibit a rather featureless growth-morphology throughout the entire coating thickness. The impact with the heavy W or Nb atoms leads to an extended, initially featureless growth-morphology close to the Si substrate interface [44,45]. Cr promotes the formation of crystalline Al_2O_3 and thus, even directly on Si substrates (with their native amorphous oxide surface) crystalline regions can form.

TEM investigations (Fig. 6d) of the coatings developed with the 2 at.% W alloyed target on the other hand clearly show an extended initial featureless growth-morphology region directly at the interface to the Si substrate. This is also reflected by the structural XRD analysis indicating an increased X-ray amorphous phase fraction, which is even more pronounced for the coatings prepared with the 5 at.% W alloyed Al target.

Coatings obtained with the Nb microalloyed targets show XRD patterns comparable to those obtained with the W microalloyed targets. The TEM investigations (Fig. 6e) also show an extended featureless growth-morphology region close to the Si substrate, followed by a more crystalline region. This is confirmed by SAED investigations showing basically γ-Al_2O_3 (not shown).

An EDS line-scan (in growth direction), Fig. 6f, indicates that particularly the featureless interface-near region contains a higher W content, confirming that the crystallization is disturbed by W. In the featureless growth-morphology region also the Si content is slightly higher.

Despite the featureless growth-morphology regions, low W containing coatings (obtained from the $Al_{0.98}W_{0.02}$ target) still have a high hardness of 28.3 GPa, even slightly above that of the coating prepared from the unalloyed Al target (having 26.8 GPa), Fig. 7a. The coatings prepared with the 2 at.% Mo or Nb alloyed targets have slightly lower hardness, whereas those sputtered with the Cr alloyed targets exhibit the highest hardness of up to 30.0 GPa. The coatings developed with the 5 at.% Nb, Mo, or W alloyed targets exhibit the lowest hardness (below 14 GPa). Interestingly here is in particular the hardness of the coatings obtained from the 2 and 5 at.% Mo alloyed Al target. While both coatings show the same Mo content (below 0.3 at.%) and also their oxygen content is similar (~58.5 at.%), Fig. 4, their hardness is

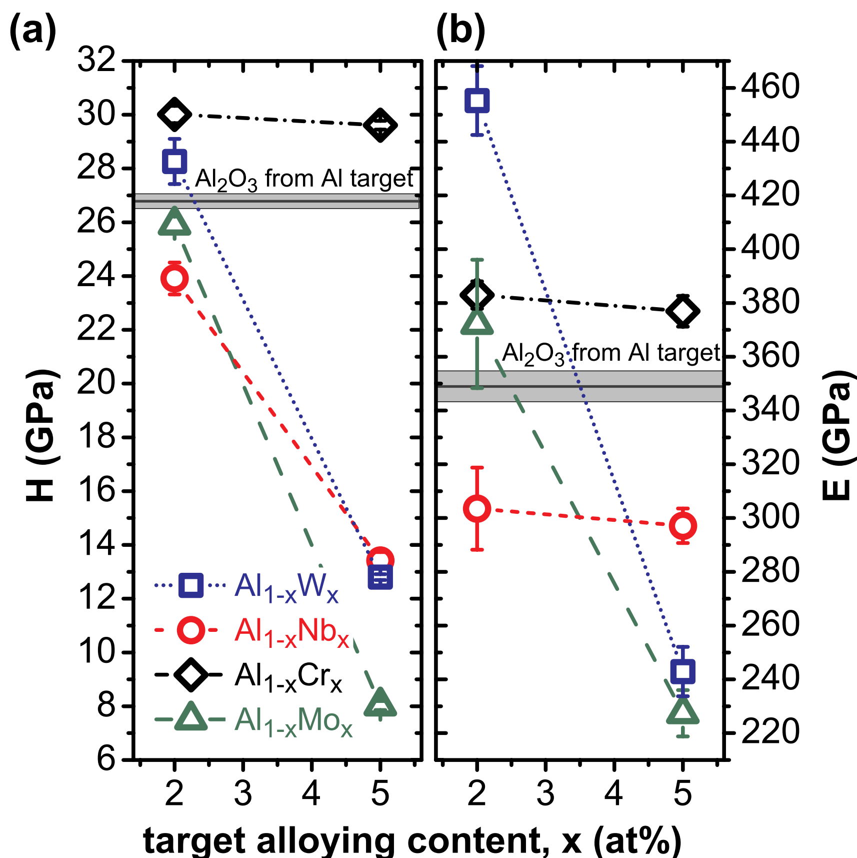

Fig. 7. (a) Hardness H and (b) indentation modulus E of our coatings prepared with $Al_{1-x}Cr_x$, $Al_{1-x}Mo_x$, $Al_{1-x}W_x$, and $Al_{1-x}Nb_x$ targets with 2 and 5 at.% alloying content (f_{O2} = 38% for the $Al_{1-x}W_x$ targets and 31% for the others).

completely different with either 25.9 or 8.0 GPa. This however agrees with the above-mentioned formation of volatile Mo-oxides during growth of the film. The higher the amount of such volatile species during growth of our films, the higher is the volume fraction of thereby disturbed growth regions within the coatings. The more Mo species arrive on the growing films (from higher Mo containing targets) the higher is the fraction of volatile oxides and the higher is the interference with the nucleation and growth process of the Al_2O_3-based film. This will lead to dramatically reduced mechanical properties, which is reflected by the massive decline in hardness (Fig. 7a) as well as indentation modulus (Fig. 7b).

As Cr is the only microalloying element (from those studied here) to form also oxides with a corundum-type crystal structure, able to form solid solutions with Al_2O_3 [33–35], it is not surprising that the Cr containing coatings remain hard even when increasing the Cr content (contrary to the other microalloying elements). The indentation modulus of our coatings follows the trend of their hardness (Fig. 7b). However, noteworthy is that the indentation modulus for our coatings prepared from the 2 at.% W alloyed target is the highest with 455 GPa, which is 106 GPa above that of the coating prepared from the unalloyed Al target.

The residual biaxial compressive stresses of our Al_2O_3-based coatings are similar with −1.6 GPa when using the unalloyed Al target or the 2 at.% Mo, Cr, or Nb alloyed targets. The coatings prepared from the 2 at.% W alloyed targets exhibit only −0.8 GPa compressive stresses. When using the 5 at.% alloyed Al targets, the compressive residual stresses increase to −3.2 GPa for coatings obtained from $Al_{0.95}Cr_{0.05}$ targets, but decrease to −0.2 GPa for coatings obtained from $Al_{0.95}W_{0.05}$ and $Al_{0.95}Nb_{0.05}$ targets, and stay at almost −1.6 GPa for the coatings obtained from $Al_{0.95}Mo_{0.05}$ targets. In general, this highlights the positive effect of rather small amounts of W on the mechanical properties of Al_2O_3, as the small hardness increase (from 26.8 to 28.3 GPa) is not due to an increase in compressive stresses.

4. Conclusion

The reactive DC sputtering process of alumina coatings in O_2 containing atmospheres from Al targets can be improved by microalloying these targets with Cr, Mo, or W. These substantially reduce severe arcing events at the target. Most effective to reduce also minor arcing events (which are not detected by the generators) is the alloying with Cr, which is also able to directly promote the formation of crystalline regions at the Si substrate surface. This is not the case for Nb but especially W, which leads to extended amorphous-like growth regions (notably for higher Nb and W contents). Mo has a special impact on the growth morphology, as most of the arriving Mo species (at the substrate and growing film) form volatile Mo-oxides. Therefore, the Mo content within the films is below 0.3 at.%, even when using the higher Mo alloyed targets (with 5 at.% Mo). These volatile Mo-oxides interrupt the nucleation and growth process of the coatings, leading to underdense growth morphologies, notably when prepared from the 5 at.% Mo alloyed targets, as thereby a higher fraction of volatile oxides form. Therefore, these coatings are also the softest (with 8.0 GPa) and exhibit the smallest indentation modulus (225 GPa) among all coatings studied.

Primarily when using the 2 at.% W alloyed Al targets, the obtained Al_2O_3-based coatings grow with a relatively high rate (R = 6.0 nm/min), exhibit a high hardness (28.3 GPa), high indentation modulus (455 GPa), and low compressive stresses (−0.8 GPa). The corresponding values for coatings prepared from unalloyed Al targets are R = 4.9 nm/min, H = 26.8 GPa, E = 349 GPa, and σ = −1.6 GPa. Using the higher W alloyed targets (with 5 at.% W) leads to a much higher growth rate (9.6 nm/min), but lower mechanical properties of

the thereby obtained Al_2O_3-based films, with H = 12.8 GPa and E = 243 GPa, because the X-ray amorphous phase fraction increases. The mechanical properties of the films prepared with the 2 and 5 at.% Cr alloyed targets (which provide the most stable deposition conditions in the O_2 containing atmosphere) are with H ~30.0 GPa and E ~380 GPa slightly above those of the Al_2O_3 coatings prepared from the unalloyed target, in agreement with their higher well-developed crystalline phase fraction as suggested by the XRD and TEM investigations.

Based on our results we can conclude that microalloying Al targets with W or Cr fundamentally improves the process conditions – reduced arcing events at the target and shifting the onset of the target poisoning regime to higher O_2/(Ar + O_2) flow-rate-ratios – and the mechanical properties of the thereby prepared Al_2O_3-based coatings.

CRediT author statement

Bernhard Kohlhauser: Investigation, Writing - original draft.
Helmut Riedl: Data curation, Supervision.
Christian Martin Koller: Investigation, Visualization.
Valentina Paneta: Investigation.
Szilárd Kolozsvári: Validation.
Paul H. Mayrhofer: Conceptualization, Methodology, Resources, Writing - review & editing, Supervision, Project administration, Funding acquisition.

Declaration of competing interest

The authors declare that they have no known competing financial interests or personal relationships that could have appeared to influence the work reported in this paper.

Acknowledgement

This work was funded by the Austrian COMET Program (project K2 XTribology, no. 849109 and project K2 InTribology, no. 872176) and has been carried out at the TU Wien and Excellence Centre for Tribology. The authors acknowledge the use of the X-ray center (XRC) and USTEM at TU Wien. Support by the Swedish Research Council (Contract No. 821-2012-5144) and the Swedish Foundation for Strategic Research (Contract No. RIF14-0053) supporting accelerator operation is gratefully acknowledged. Plansee Composite Materials GmbH is acknowledged for support with target materials.

References

[1] G. Balakrishnan, P. Kuppusami, S.T. Sundari, R. Thirumurugesan, V. Ganesan, E. Mohandas, D. Sastikumar, Structural and optical properties of γ-alumina thin films prepared by pulsed laser deposition, Thin Solid Films 518 (2010) 3898–3902.
[2] S. Zhu, F. Wang, H. Lou, W. Wu, Reactive sputter deposition of alumina films on superalloys and their high-temperature corrosion resistance, Surf. Coat. Technol. 71 (1995) 9–15.
[3] R. Cremer, M. Witthaut, K. Reichert, D. Neuschütz, Surface and interface analysis of PVD Al-O-N and γ-Al2O3 diffusion barriers, Fresenius J. Anal. Chem. 365 (1999) 158–162.
[4] R. Cremer, M. Witthaut, K. Reichert, M. Schierling, D. Neuschütz, Thermal stability of Al-O-N PVD diffusion barriers, Surf. Coat. Technol. 108–109 (1998) 48–58.
[5] K. Bobzin, N. Bagcivan, P. Immich, M. Ewering, Thermal investigation of Al2O3 thin films for application in cutting operations, Adv. Eng. Mater. 11 (2009) 590–594.
[6] M. Åstrand, T.I. Selinder, F. Fietzke, H. Klostermann, PVD-Al2O3-coated cemented carbide cutting tools, Surf. Coat. Technol. 188–189 (2004) 186–192.
[7] K. Bobzin, E. Lugscheider, M. Maes, C. Piñero, Relation of hardness and oxygen flow of Al2O3 coatings deposited by reactive bipolar pulsed magnetron sputtering, Thin Solid Films 494 (2006) 255–262.
[8] V. Edlmayr, M. Moser, C. Walter, C. Mitterer, Thermal stability of sputtered Al2O3 coatings, Surf. Coat. Technol. 204 (2010) 1576–1581.
[9] O. Zywitzki, G. Hoetzsch, F. Fietzke, K. Goedicke, Effect of the substrate temperature on the structure and properties of Al2O3 layers reactively deposited by pulsed magnetron sputtering, Surf. Coat. Technol. 82 (1996) 169–175.
[10] O. Zywitzki, G. Hoetzsch, Effect of plasma activation on the phase transformations of aluminum oxide, Surf. Coat. Technol. 76–77 (1995) 754–762.
[11] O. Zywitzki, G. Hoetzsch, Influence of coating parameters on the structure and properties of Al2O3 layers reactively deposited by means of pulsed magnetron sputtering, Surf. Coat. Technol. 86–87 (1996) 640–647.
[12] T. Kohara, H. Tamagaki, Y. Ikari, H. Fujii, Deposition of α-Al2O3 hard coatings by reactive magnetron sputtering, Surf. Coat. Technol. 185 (2004) 166–171.
[13] H. Bolt, F. Koch, J.L. Rodet, D. Karpov, S. Menzel, Al2O3 coatings deposited by filtered vacuum arc - characterization of high temperature properties, Surf. Coat. Technol. 116–119 (1999) 956–962.
[14] G. Zhou, L. Wang, X. Wang, Y. Yu, Deposition of nanostructured crystalline alumina thin film by twin targets reactive high power impulse magnetron sputtering, Appl. Surf. Sci. 455 (2018) 310–317.
[15] A. Schütze, D.T. Quinto, Pulsed plasma-assisted PVD sputter-deposited alumina thin films, Surf. Coat. Technol. 162 (2003) 174–182.
[16] S. Berg, T. Nyberg, Fundamental understanding and modeling of reactive sputtering processes, Thin Solid Films 476 (2005) 215–230.
[17] S. Maniv, W.D. Westwood, Discharge characteristics for magnetron sputtering of Al in Ar and Ar/O//2 mixtures, J. Vac. Sci. Technol. 17 (1980) 743–751.
[18] K. Bobzin, N. Bagcivan, M. Ewering, Influence of different pulse parameters on the deposition of Al2O3, Mater. wis. Werkstofftech. 41 (2010) 670–674.
[19] I. Safi, Recent aspects concerning DC reactive magnetron sputtering of thin films: a review, Surf. Coat. Technol. 127 (2000) 203–219.
[20] T. Nyberg, S. Berg, U. Helmersson, K. Hartig, Eliminating the hysteresis effect for reactive sputtering processes, Appl. Phys. Lett. 86 (2005) 164106.
[21] D. Severin, O. Kappertz, T. Kubart, T. Nyberg, S. Berg, A. Pflug, M. Siemers, M. Wuttig, Process stabilization and increase of the deposition rate in reactive sputtering of metal oxides and oxynitrides, Appl. Phys. Lett. 88 (2006) 161504.
[22] W.D. Sproul, D.J. Christie, D.C. Carter, Control of reactive sputtering processes, Thin Solid Films 491 (2005) 1–17.
[23] E. Wallin, U. Helmersson, Hysteresis-free reactive high power impulse magnetron sputtering, Thin Solid Films 516 (2008) 6398–6401.
[24] E. Särhammar, S. Berg, T. Nyberg, Hysteresis-free high rate reactive sputtering of niobium oxide, tantalum oxide, and aluminum oxide, J. Vac. Sci. Technol. A 32 (2014) 041517.
[25] W.D. Sproul, M.E. Graham, M.S. Wong, S. Lopez, D. Li, R.A. Scholl, Reactive direct current magnetron sputtering of aluminum oxide coatings, J. Vac. Sci. Technol. A 13 (1995) 1188–1191, https://doi.org/10.1116/1.579859.
[26] S. Berg, A.M. Barklund, B. Gelin, C. Nender, I. Katardjiev, Atom assisted sputtering yield amplification, J. Vac. Sci. Technol. A 10 (1992) 1592–1596.
[27] S. Berg, I.V. Katardjiev, Preferential sputtering effects in thin film processing, J. Vac. Sci. Technol. A 17 (1999) 1916–1925.
[28] T. Kubart, R.M. Schmidt, M. Austgen, T. Nyberg, A. Pflug, M. Siemers, M. Wuttig, S. Berg, Modelling of sputtering yield amplification in serial reactive magnetron co-sputtering, Surf. Coat. Technol. 206 (2012) 5055–5059.
[29] D. Depla, Z.Y. Chen, A. Bogaerts, V. Ignatova, R. De Gryse, R. Gijbels, Modeling of the target surface modification by reactive ion implantation during magnetron sputtering, J. Vac. Sci. Technol. A 22 (2004) 1524–1529.
[30] M. Austgen, D. Koehl, P. Zalden, T. Kubart, T. Nyberg, A. Pflug, M. Siemers, S. Berg, M. Wuttig, Sputter yield amplification by tungsten doping of Al2O3 employing reactive serial co-sputtering: process characteristics and resulting film properties, J. Phys. D. Appl. Phys. 44 (2011).
[31] T. Kubart, T. Nyberg, A. Pflug, M. Siemers, M. Austgen, D. Koehl, M. Wuttig, S. Berg, Modelling of sputtering yield amplification effect in reactive deposition of oxides, Surf. Coat. Technol. 204 (2010) 3882–3886.
[32] J. Paulitsch, R. Rachbauer, J. Ramm, P. Polcik, P.H. Mayrhofer, Influence of Si on the target oxide poisoning during reactive arc evaporation of $(Al,Cr)_2O_3$ coatings, Vacuum 100 (2014) 29–32, https://doi.org/10.1016/j.vacuum.2013.06.008.
[33] J.M. Andersson, E. Wallin, U. Helmersson, U. Kreissig, E.P. Münger, Phase control of Al2O3 thin films grown at low temperatures, Thin Solid Films 513 (2006) 57–59.
[34] M. Ristić, S. Popović, S. Musić, Structural properties of the system Al2O3-Cr2O3, Mater. Lett. 16 (1993) 309–312.
[35] Y. Kitaoka, K. Nakamura, T. Akiyama, T. Ito, Structural stability and electronic properties in Al2O3–Cr2O3 mixed crystal, J. Cryst. Growth 362 (2013) 42–44.
[36] R.L. Merlino, Understanding Langmuir probe current-voltage characteristics, Am. J. Phys. 75 (2007) 1078–1085.
[37] M. Mayer, S. Möller, M. Rubel, A. Widdowson, S. Charisopoulos, T. Ahlgren, E. Alves, G. Apostolopoulos, N.P. Barradas, S. Donnelly, S. Fazinić, K. Heinola, O. Kakuee, H. Khodja, A. Kimura, A. Lagoyannis, M. Li, S. Markelj, M. Mudrinic, P. Petersson, I. Portnykh, D. Primetzhofer, P. Reichart, D. Ridikas, T. Silva, S.M. Gonzalez de Vicente, Y.Q. Wang, Ion beam analysis of fusion plasma-facing materials and components: facilities and research challenges, Nucl. Fusion. 60 (2019) 25001, https://doi.org/10.1088/1741-4326/ab5817.
[38] P. Ström, P. Petersson, M. Rubel, G. Possnert, A combined segmented anode gas ionization chamber and time-of-flight detector for heavy ion elastic recoil detection analysis, Rev. Sci. Instrum. 87 (2016) 103303.
[39] H. Lasfargues, T. Glechner, C.M. Koller, V. Paneta, D. Primetzhofer, S. Kolozsvári, D. Holec, H. Riedl, P.H. Mayrhofer, Non-reactively sputtered ultra-high temperature Hf-C and Ta-C coatings, Surf. Coat. Technol. 309 (2017) 436–444, https://doi.org/10.1016/j.surfcoat.2016.11.073.
[40] W.C. Oliver, G.M. Pharr, Measurement of hardness and elastic modulus by instrumented indentation: advances in understanding and refinements to methodology, J. Mater. Res. 19 (2004) 3–20.
[41] J.D. Wilcock, D.S. Campbell, A sensitive bending beam apparatus for measuring the stress in evaporated thin films, Thin Solid Films 3 (1969) 3–12, https://doi.org/10.1016/0040-6090(69)90107-2.
[42] H. Asanuma, F.F. Klimashin, P. Polcik, S. Kolozsvári, H. Riedl, P.H. Mayrhofer, Impact of lanthanum and boron on the growth, thermomechanical properties and

oxidation resistance of Ti–Al–N thin films, Thin Solid Films 688 (2019) 137239 1–8, https://doi.org/10.1016/j.tsf.2019.04.014.
[43] H. Asanuma, F.F. Klimashin, P. Polcik, S. Kolozsvári, H. Riedl, P.H. Mayrhofer, Hard Ti-Al-N endowed with high heat-resistance through alloying with Ta and Ce, Surf. Coat. Technol. 372 (2019) 26–33, https://doi.org/10.1016/j.surfcoat.2019.05.018.
[44] M.G.J. Müller, F. Nahif, J. Mayer, J.M. Schneider, Transmission electron microscopy investigation of the effect of Si alloying on the thermal stability of amorphous alumina thin films deposited by filtered cathodic arc deposition, Surf. Coat. Technol. (2014), https://doi.org/10.1016/j.surfcoat.2014.07.088.
[45] K. Bobzin, N. Bagcivan, M. Müller, M. Ewering, R.H. Brugnara, Thermal stability of silicon-doped Al2O3 PVD coatings, Mater. wis. Werkstofftech. 44 (2013) 679–683.